Available online at www.sciencedirect.com
ScienceDirect
Journal of Catalysis 249 (2007) 162–173
JOURNAL OF CATALYSIS
www.elsevier.com/locate/jcat

A detailed study of the activity and deactivation of zeolites in hybrid Co/SiO_2-zeolite Fischer–Tropsch catalysts

Agustín Martínez [a,*], Joan Rollán [a], Maria A. Arribas [a], Henrique S. Cerqueira [b], Alexandre F. Costa [a], Eduardo Falabella S.-Aguiar [b]

[a] *Instituto de Tecnología Química, UPV-CSIC, Avda. de los Naranjos s/n, 46022 Valencia, Spain*
[b] *Petrobras, Centro de Pesquisas e Desenvolvimento Leopoldo A. Miguez de Mello (CENPES), Av. Jequitibá 950, Cidade Universitária, Ilha do Fundão, 21941-598 Rio de Janeiro, RJ, Brazil*

Received 12 March 2007; accepted 9 April 2007

Available online 4 June 2007

Abstract

The influence of the zeolite pore topology and acidity in hybrid catalysts comprising a physical mixture of a silica-supported cobalt (20 wt% Co) active in the Fischer–Tropsch (FT) synthesis and an acidic zeolite active in cracking under typical FT synthesis conditions (250 °C, 2.0 MPa, and $H_2/CO = 2$) has been studied. The zeolite cracked the primary C_{13+} long-chain *n*-paraffins formed on the Co catalyst to mainly gasoline-range branched products. The yield of branched products declined with TOS due to the accumulation of carbonaceous deposits (coke) on the zeolite. The amount of coke retained in spent zeolites correlated well with the observed deactivation rate and both increased with the zeolite pore dimensions, i.e. HZSM-5 < HMOR < HBeta < USY, but was little affected by zeolite acidity (USY-500 ∼ USY-720). Coke molecules predominantly comprised 2- and 3-ring aromatics in large pore zeolites, while it was mainly of paraffinic nature in the most stable HZSM-5. Aromatic coke is likely formed from light olefins produced in the FT synthesis through consecutive oligomerization, cyclization, and dehydrogenation reactions. Independent *n*-hexadecane cracking experiments performed under simulated FT conditions revealed that water, a primary product of the FT reaction, reduces the cracking activity of the zeolite by competing with the *n*-alkane feed molecules for adsorption on the Brønsted acid sites but has no appreciable effect on its stability with TOS.

Keywords: Fischer–Tropsch; Hybrid catalysts; Silica-supported cobalt; Zeolite acidity; Zeolite pore structure; Deactivation; Coke

1. Introduction

The Fischer–Tropsch (FT) synthesis is an attractive route to produce high-quality liquid fuels from alternative sources to petroleum, such as natural gas, coal, and biomass via conversion of syngas (mixture of CO and H_2) over cobalt or iron based catalysts. During the last decades significant improvements were made both on the reactor [1] and catalyst technologies [2,3]. With iron catalysts and process temperatures close to 350 °C, the main products are premium petrochemical naphtha and α-olefins. With cobalt-based catalysts and reaction temperatures in the range of 210–250 °C and after an upgrading (hydrocracking and hydrodewaxing) step, the main products are premium diesel (cetane number higher than 70 and virtually no S or aromatic compounds), food grade paraffin and specialty lubricants.

Despite all those advantages, the production of liquid fuels by the FT process suffers from two main constraints. On one hand, the polymerization-type kinetics of the FT reaction results in a statistical distribution of hydrocarbons (from methane to waxy products) known as Anderson–Schulz–Flory or ASF distribution characterized by the parameter α (chain growth probability). The ASF kinetics of the FT reaction imposes a limit to the maximum selectivity attainable for a given hydrocarbon fraction (i.e., 48% for gasoline-range products). On the other hand, the linear structure of the FT hydrocarbons (mostly *n*-paraffins) results in a too low quality fuel to be directly blended into the gasoline and diesel pools due to their low octane numbers and poor cold flow properties, respectively. There are different possibilities to improve the selectivity and qual-

* Corresponding author. Fax: +34 963 877 809.
E-mail address: amart@itq.upv.es (A. Martínez).

0021-9517/$ – see front matter
doi:10.1016/j.jcat.2007.04.012

ity of the primary FT products using down-stream conversion units. For instance, olefinic and oxygenated FT products can be upgraded to high-octane gasoline rich in isoparaffins and aromatics over a ZSM-5 zeolite catalyst [4], while heavy *n*-paraffins (waxes) can be selectively hydrocracked to produce diesel fuel with high cetane number and improved cold flow properties [5]. Moreover, the FT waxes have shown high potential as feedstock for catalytic cracking units (FCC) to produce high-octane gasoline with high content of isoparaffins and almost no aromatics, as well as light olefins which are valuable raw materials for petrochemistry [6,7].

An interesting alternative to the above two-stage processing to circumvent the selectivity and quality limitations of the FT process is the use of hybrid or composite catalysts comprising a FT base catalyst and a co-catalyst containing the appropriate functionality to convert in a single-stage the primary FT products into the desired compounds. Thus, the combination of an iron-based FT catalyst displaying high selectivity to short-chain α-olefins and oxygenates with ZSM-5 [8–12] or HY [13] zeolites results in an enhanced gasoline selectivity and an increased concentration of high-octane branched and aromatic hydrocarbons by promoting oligomerization, cracking, isomerization, and aromatization reactions on the zeolite acid sites at the relatively high temperatures applied. A gradual loss of the zeolite activity by coking was always observed during the single-stage operation with hybrid catalysts. In this respect, we recently showed that decreasing the crystallite size and adding a small amount of a noble metal (e.g., Pd) to the ZSM-5 zeolite significantly improves the stability of the zeolite co-catalyst against deactivation [14]. On the other hand, gasoline-range isoparaffins also can be produced in a single reactor using hybrid catalysts by combining a Co-based FT catalyst (e.g., Co/SiO_2) with an acidic or bifunctional zeolite co-catalyst [15–17]. In this case, the primary waxy products formed on the Co catalyst are cracked/hydrocracked into mainly branched hydrocarbons with limited formation of aromatics, a less desirable component in reformulated gasolines due to environmental concerns.

In this context, the objective of the present work was to study the influence of the zeolite pore topology (USY, Beta, Mordenite, and ZSM-5) on the activity of hybrid catalysts containing Co/SiO_2 and an acidic zeolite component in producing gasoline-range branched hydrocarbons directly from syngas. The effect of the zeolite acidity was also studied by using two USY samples with different silica-to-alumina framework and extra-framework compositions. The deactivation of the different zeolites plays a key role in the process, justifying a detailed study of the amount and nature of the coke molecules retained in the spent zeolites, which was also done in the present work.

2. Experimental

2.1. Catalyst preparation

A silica-supported cobalt catalyst (Co/SiO_2) with a nominal Co loading of 20 wt% was used as the base Fischer–Tropsch component. This material was prepared by impregnation of a commercial amorphous SiO_2 (Fluka, silica gel 100, BET = 387 m^2/g, PV = 0.8 cm^3/g) with an excess of an aqueous solution containing the required amount of $Co(NO_3)_2{\cdot}6H_2O$ (Aldrich, 98%). After the mixture was stirred for 1 h at ambient temperature, the water solvent was eliminated by rotavaporation. Then the solid was dried in an oven at 60 °C overnight, and finally calcined at 300 °C for 10 h in a muffle.

To study the influence of the zeolite acidity and topology on the performance of the hybrid Co/SiO_2 + zeolite mixtures, five commercial samples composing four different structures were purchased from Zeolyst International: USY-500 (CBV500), USY-720 (CBV720), HBeta (CP811), HMOR (CBV20A), and HZSM-5 (CBV3020). The two USY samples differed in their framework and extra-framework Si/Al ratios and thus in their acidity. The CBV500, CBV712, and CBV20A samples, which were originally in ammonium form, were submitted to a calcination step at 500 °C for 3 h to obtain the protonic form.

The hybrid catalysts were obtained by physically mixing 1.0 g of the base Co/SiO_2 and 1.0 of the H-zeolite, both previously pressed, crushed, and sieved to a particle size of 0.25–0.42 mm.

2.2. Characterization techniques

The cobalt content in the Co/SiO_2 catalyst was determined by atomic absorption spectrophotometry (AAS) in a Varian Spectra A-10 Plus apparatus. Textural properties were obtained from the N_2 adsorption isotherms at −196 °C in a Micromeritics ASAP 2000 equipment. The specific surface area was calculated by the BET method and the micropore volume by the *t*-plot approach. Before the adsorption measurements, the samples were degassed at 400 °C for 24 h.

X-ray diffraction (XRD) patterns were obtained at room temperature in a Phillips X'pert diffractometer using monochromatized CuK_α radiation. The average particle size of Co_3O_4 in the calcined Co/SiO_2 catalyst was estimated from Scherrer's equation using the most intense reflection of Co_3O_4 crystallites at $2\theta = 36.9°$. The Co_3O_4 particle size in the calcined sample was then converted to the cobalt metal diameter in the reduced catalyst by considering the relative molar volumes of Co^0 and Co_3O_4 using the equation [18]

$$d(Co^0) = 0.75 \cdot d(Co_3O_4).$$

Then the Co^0 metal dispersion was estimated from $d(Co^0)$ by assuming a spherical geometry of the metal particles with uniform site density of 14.6 atoms per nm^2 using the following equation [19,20]:

$$D = 96/d,$$

where D is the % Co^0 dispersion and d is the mean particle size of Co^0 in nm.

The reduction profile of cobalt in Co/SiO_2 was studied by H_2-TPR in a Micromeritics Autochem 2910 device. About 30 mg of the calcined catalyst was initially flushed with 30 cm^3/min of Ar at room temperature for 30 min, and then a mixture of 10 vol% of H_2 in Ar was passed through the catalyst at a total flow rate of 50 cm^3/min while the temperature

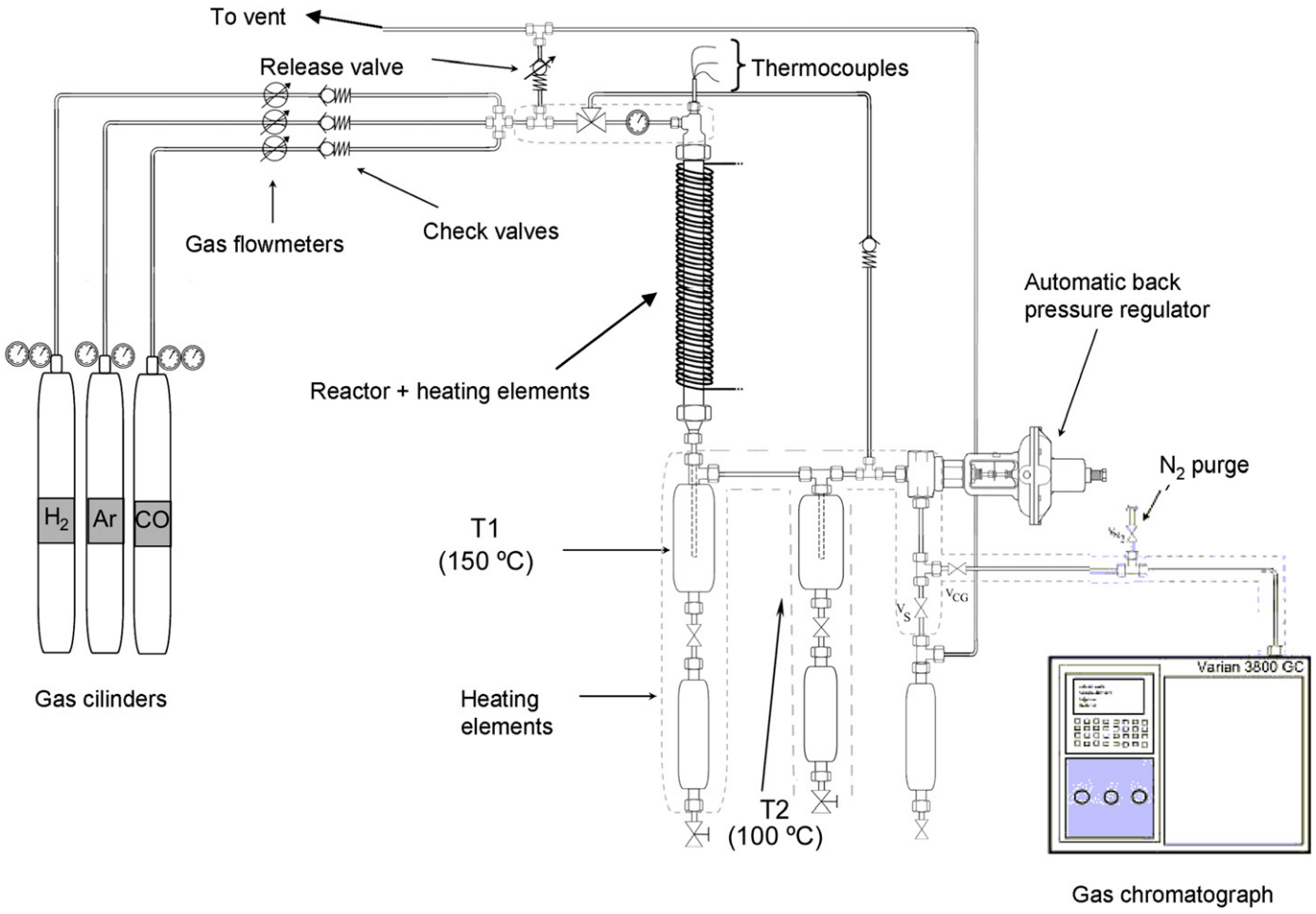

Fig. 1. Scheme of the reaction system used for the catalytic experiments.

was increased up to 900 °C at a rate of 10 °C/min. The H_2 consumption rate was monitored in a thermal conductivity detector (TCD) previously calibrated using the reduction of CuO as standard. The extent of cobalt reduction was also determined by TPR after submitting the calcined Co/SiO_2 to the same reduction treatment applied just before the catalytic tests (400 °C, 10 h), as described previously [21].

Finally, the acidity of the H-zeolites was determined by IR spectroscopy with the adsorption of pyridine and subsequent desorption and temperature increase (250–400 °C) in an FTIR Nicolet 710 device following the experimental procedure reported elsewhere [22]. The amount of pyridine retained on Brønsted and Lewis acid sites was calculated from the integrated absorbances of the IR bands at ca. 1545 and 1450 cm^{-1}, respectively, using the extinction coefficients given by Emeis [23].

2.3. Catalytic experiments

2.3.1. Fischer–Tropsch synthesis

The Fischer–Tropsch synthesis was carried out in a downflow fixed-bed stainless steel reactor. A scheme of the reaction system, including the feed section, FT reactor, product condensation, and online GC analysis, is presented in Fig. 1. In a typical experiment, the reactor was loaded with 2.0 g of hybrid catalyst (1.0 g of Co/SiO_2 and 1.0 g of H-zeolite) diluted with silicon carbide up to a constant bed volume of 6.4 cm^3. Before the catalytic experiments, a flow of pure H_2 was passed through the reactor at atmospheric pressure and 400 °C for 10 h to promote the reduction of cobalt in the Co/SiO_2 base component. Then the temperature was lowered to 100 °C under the flow of H_2, and subsequently a flow (250 cm^3/min) of a mixture of CO, H_2, and Ar (CO:H_2:Ar volume ratio of 3:6:1, with Ar the internal standard) was established, corresponding to a gas hourly space velocity (GHSV) of 13.5 $l_{syngas}/(g_{cat}\,h)$ referred to the FT catalyst and the reaction pressure slowly increased up to 2.0 MPa. Then the temperature was raised at a rate of 4 °C/min up to 250 °C. The temperature in the catalyst bed was controlled to 250 ± 1 °C by means of two independent heating zones, with the corresponding temperature controllers connected to thermocouples located in different positions inside the catalytic bed.

During the reaction, the reactor effluent passed through two consecutive traps heated at 150 and 100 °C, respectively, and maintained at the reaction pressure (2.0 MPa) to condense the heaviest hydrocarbons (waxes). The product stream leaving the second trap (unreacted H_2 and CO, CO_2, water, alcohols, and hydrocarbons up to C_{15}–C_{20}) was depressurized and analyzed online. Gas chromatography (GC) data were collected at peri-

Table 1
Experimental conditions used in the *n*-hexadecane cracking experiments (reaction temperature and total pressure were kept constant at 250 °C and 2.0 MPa, respectively)

Experiment	Partial pressure (MPa)				Catalyst (g)		Activation conditions
	n-C_{16}	H_2O	H_2	N_2	Zeolite	Co/SiO_2	
A[a]	0.24	–	0.70	1.06	–	–	None
B	0.24	–	0.70	1.06	1.0	–	None
C	0.24	–	–	1.76	1.0	–	None
D	0.24	–	0.70	1.06	–	1.0	Reduction at 400 °C/10 h
E[b]	0.24	–	0.70	1.06	1.0	1.0	Reduction at 400 °C/10 h
F[b]	0.24	0.63	0.70	0.43	1.0[a]	1.0	Reduction at 400 °C/10 h

[a] Inert silicon carbide was loaded in the reactor.
[b] Physical mixture of the two catalyst components.

odic intervals with a Varian 3800 chromatograph equipped with three columns and two detectors. Details of the GC analyses have been provided elsewhere [21,24]. Carbon mass balances performed at the end of the experiments, including the amount of waxy products collected in the traps, were quite satisfactory ($100 \pm 2\%$). Product yields and selectivities are given on a carbon basis.

At the end of each run (about 15–16 h time on stream [TOS]), the reactor was depressurized, and the syngas flow was swapped to a 100 cm^3/min of a H_2/Ar mixture (50:50 by volume) at the same temperature (250 °C) for about 12 h, to desorb weakly adsorbed hydrocarbons from the Co/SiO_2 and the zeolite solids. Then the system was cooled to ambient temperature, the H_2/Ar gas flow was stopped, and the solid catalysts were removed from the reactor. The zeolite was carefully physically separated from the Co/SiO_2 and SiC components for determination of the amount and nature of the hydrocarbons retained (generally denoted as coke). The total amount of carbon in the spent zeolites was then determined by elemental analysis in a Fisons EA1108 CHNS-O analyzer. The nature of the coke molecules was identified using the methodology developed by Magnoux et al. [25]. Briefly, the coked zeolites were first submitted to a Soxhlet extraction treatment using dichloromethane (CH_2Cl_2) as a solvent for about 20 h. The quantity of organic residue remaining after complete evaporation of the solvent in a rotary evaporator was designated type I soluble coke. The coke remaining in the zeolite after the Soxhlet extraction was liberated by dissolving the zeolite in a 40% HF solution at room temperature. Then CH_2Cl_2 was added to dissolve the soluble part of the liberated coke and the amount of residue remaining after complete evaporation of the solvent, designated type II soluble coke. In all cases, the fraction of insoluble coke was found to be insignificant by comparing the weight of total soluble coke with the total amount of carbon determined by elemental analysis. Types I and II soluble coke were dissolved in CH_2Cl_2 and analyzed by GC-MS, using an Agilent 6890N gas chromatograph coupled with an Agilent 5973N mass selective detector, to identify the nature of the coke molecules retained in the spent zeolites.

2.3.2. Cracking of n-hexadecane

Independent experiments were performed using *n*-hexadecane (Sigma, 99%) as model molecule representative of the long-chain *n*-paraffins produced during the FT synthesis to gain insight into the cracking behavior of the zeolite in the hybrid catalysts. The reactions were carried out in a continuous fixed-bed stainless steel reactor under conditions identical those encountered by the zeolite in the FT synthesis experiments except with the absence of CO (because this molecule is not expected to affect the cracking behavior of zeolite). The reaction temperature and the total pressure were kept constant at 250 °C and 2.0 MPa, respectively, in all cracking experiments. Six different experiments were performed to elucidate the role of H_2, water, and the presence of the base Co/SiO_2 FT catalyst on the cracking activity and stability of the zeolite during FT synthesis. The feed and catalyst bed compositions and activation conditions applied in the different cracking experiments are summarized in Table 1. The zeolite used in the n-C_{16} cracking study was HZSM-5.

n-Hexadecane and water were independently fed to the reactor by high-precision HPLC pumps (Gilson 305) at flow rates of 9.4 and 2.0 g/h, respectively. Hydrogen and nitrogen (balance inert gas) were fed at the desired flow rate using mass flow controllers (Brooks Instrument). The stream leaving the reactor was depressurized and analyzed online in a gas chromatograph (Varian Star 3800 CX) equipped with a capillary column (Petrocol DH 50.2TM, 50 m × 0.2 mm, 0.5 μm film, Supelco) and a flame ionization detector.

Table 2
Properties of the base Co/SiO_2 catalyst

Sample	Co (wt%)	BET (m^2/g)	$d(Co_3O_4)$ (nm)	Co^0 dispersion (%)	Degree of reduction[a] (%)
Co/SiO_2	19.5	300	13.9	9.2	95

[a] Estimated from H_2-TPR after reduction in H_2 flow at 400 °C for 10 h.

3. Results and discussion

3.1. Characterization of materials

3.1.1. Co/SiO2 base catalyst

The main properties of the base Co catalyst are given in Table 2. The cobalt content in the base Co/SiO_2 catalyst determined by AAS was 19.5 wt%. The BET surface area of the calcined Co catalyst was 300 m^2/g. The spinel Co_3O_4 was the only crystalline Co phase detected by XRD on calcination at

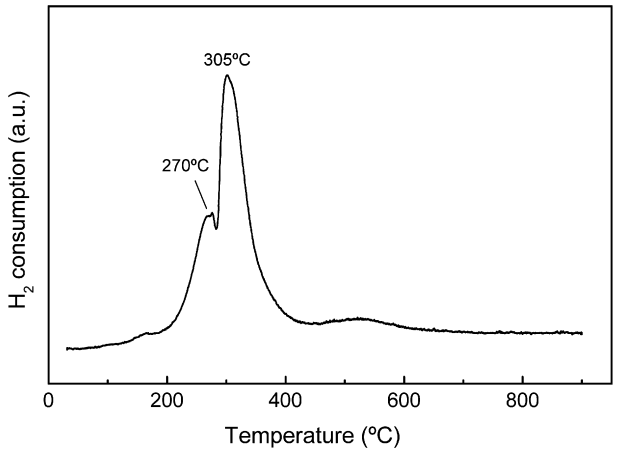

Fig. 2. H_2-TPR profile for the base Co/SiO_2 catalyst.

300 °C. The mean particle size of the supported Co_3O_4 phase was ca. 13.9 nm, as estimated by XRD, corresponding to a 9.2% dispersion of Co^0 species in the reduced catalyst.

The TPR profile of Co/SiO_2 (Fig. 2) indicates high reducibility of the supported Co_3O_4 phase, as expected from the relatively high Co loading and the weak interaction between the cobalt nitrate precursor and the silica surface [21,26,27]. In fact, the extent of reduction of Co_3O_4 in our Co/SiO_2 sample after reduction at 400 °C for 10 h (the same reduction conditions applied before the catalytic studies) estimated by TPR was 95% (Table 2).

3.1.2. Acidic zeolite co-catalysts

The chemical composition and textural properties of the different H-zeolites used as acid co-catalysts are summarized in Table 3. It can be seen that USY-500 has both lower framework and bulk Si/Al ratios than USY-720, indicating that the latter was more severely dealuminated and that part of the generated EFAL was removed by postsynthesis treatments. The bulk Si/Al ratios for the rest of zeolites were 10 for HMOR, 12.5 for HBeta, and 15 for HZSM-5.

The acid properties derived from FTIR after ad/desorption of pyridine are shown in Table 4. Different framework and extra-framework compositions of the two USY samples resulted in significant differences in the amount and strength of the Brønsted acid sites. Thus, USY-500 with a lower framework Si/Al ratio (and thus a higher framework Al content) contained about twice the amount of Brønsted acid sites than USY-720, as estimated from the amount of pyridine retained at the desorption temperature of 250 °C. The amount of Lewis acid sites, generally associated with cationic-type extra-framework Al (EFAL) species [28], was also higher in USY-500 than in USY-720, in agreement with the lower amount of EFAL species in the latter. On the other hand, HMOR had a similar number of Brønsted acid sites as the most acidic USY-500 sample. HBeta had fewer Brønsted acid sites, but higher acid strength, than HZSM-5.

3.2. FT synthesis results on hybrid catalysts

3.2.1. CO conversion and product distribution

The change in CO conversion with TOS for the base Co/SiO_2 and the hybrid catalysts is shown in Fig. 3. As can be seen, there were no substantial differences in CO conversion between the base and the hybrid catalysts, indicating that, as expected, the metal-free H-zeolites were not active for CO hydrogenation. In all cases, CO conversion gradually decreased

Table 3
Physico-chemical characteristics of the H-zeolites

Zeolite	a_0[a] (nm)	Bulk Si/Al ratio	Surface area (m^2/g)	Pore volume (cm^3/g)	Micropore volume (cm^3/g)	Crystal size[c] (μm)
USY-500	2.453	2.6 (4.7)[b]	594	0.40	0.25	0.4–0.6
USY-720	2.428	15.0 (35.3)[b]	642	0.47	0.23	0.4–0.6
HBeta	–	12.5	598	0.84	0.18	0.1–0.2
HMOR	–	10.0	463	0.34	0.19	0.1–0.3
HZSM-5	–	15.0	388	0.28	0.11	∼0.1

[a] a_0 = unit cell size parameter obtained from XRD.
[b] Values in parentheses are the framework Si/Al atomic ratios obtained from a_0 using the Fichtner–Smittler equation.
[c] Average values given by the supplier.

Table 4
Acidity of H-zeolites as determined by FTIR of adsorbed pyridine

Zeolite	Amount of acid sites[a] (μmol/g)							
	Brønsted				Lewis			
	250 °C	350 °C	400 °C	Strong[b]	250 °C	350 °C	400 °C	Strong[b]
USY-500	436	197	131	0.300	170	123	95	0.559
USY-720	233	111	45	0.193	72	64	49	0.681
HBeta	184	148	75	0.408	190	162	153	0.805
HMOR	415	168	87	0.209	219	169	152	0.696
HZSM-5	292	205	99	0.339	107	78	72	0.673

[a] Able to retain pyridine at a given temperature.
[b] Ratio between acid sites able to retain pyridine at 400 and 250 °C.

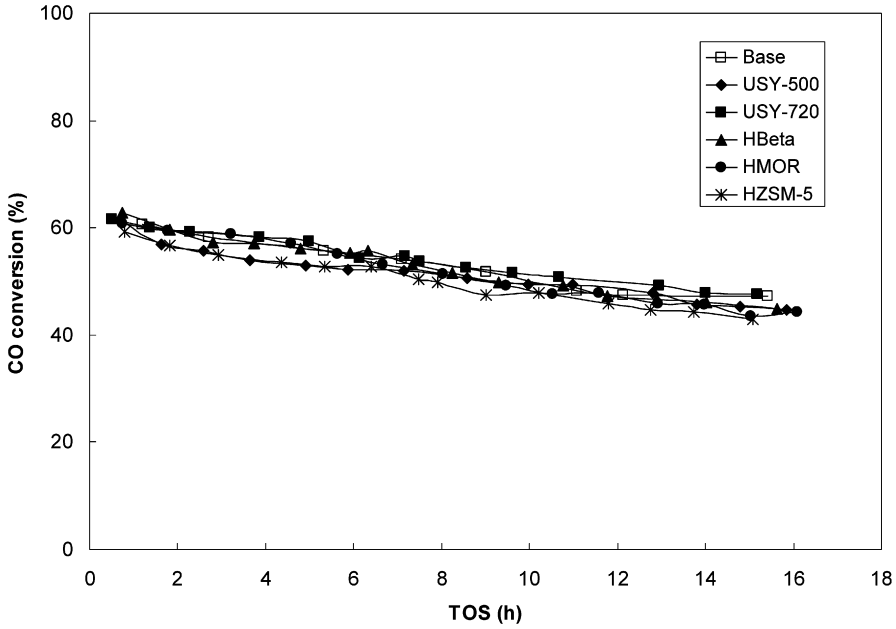

Fig. 3. CO conversion against TOS for the base and hybrid catalysts. Reaction conditions: 250 °C, 2.0 MPa, H_2/CO molar ratio of 2, GHSV of 13.5 $l_{syngas}/(g_{cat}\ h)$.

Table 5
Average hydrocarbon distribution (% C) for the base and base + zeolite hybrid catalysts for the last 7–8 h of the reaction

Hydrocarbon fraction	Base	Base + USY-500	Base + USY-720	Base + HBeta	Base + HMOR	Base + ZSM-5
C_1	11.8	12.0	11.6	11.5	11.0	11.0
C_2–C_4	10.8	12.2	13.3	13.7	14.2	14.7
C_5–C_{12}	41.0	44.4	48.6	57.3	55.8	62.2
C_{13}–C_{22}	28.3	24.9	21.3	16.4	16.8	11.0
C_{23+}	8.1	6.4	5.2	1.1	2.2	1.1

from ∼60% at ca. 0.5 h TOS to ∼45% after 15–16 h TOS. A steady deactivation with TOS is a well-known property of Co-based FT catalysts and has been generally ascribed to a decrease in the amount of accessible surface Co^0 sites resulting from a combination of different deactivating mechanisms, among which the accumulation of heavy hydrocarbons (waxes) on the catalyst surface [29] and a certain reoxidation of the smallest cobalt particles by the water byproduct during the course of the reaction [30,31] have been postulated. In some cases, an improved lifetime of the base FT catalyst has been observed for hybrid systems composing an acidic co-catalyst, which has been related to the cracking of part of the waxy products accumulated on the surface of the FT catalyst [32]. In the present case, such a beneficial effect of the addition of zeolite on the stability of the Co/SiO_2 catalyst was not observed, at least within the reaction times studied (15–16 h), even if, as will be shown after, part of the heaviest hydrocarbons formed on the base component were cracked on the zeolite acid sites. This is probably due to the relatively low amount of waxy hydrocarbons formed on the Co/SiO_2 catalyst at the reaction conditions used here (C_{23+} selectivity of 8.1% C).

Table 5 shows the hydrocarbon distributions averaged for the last 7–8 h TOS, obtained by combining the online GC analyses and the analysis of the waxy hydrocarbons accumulated in the high-pressure traps at the reactor outlet (Fig. 1) during the same period. As can be seen in Table 5, methane selectivities of around 11–12% C were obtained for the base and hybrid catalysts, confirming, as expected, that the zeolite component did not further contribute to the formation of methane by cracking at the conditions used. The main effect of the zeolite co-catalyst was seen to increase the selectivity to gasoline-range products (C_5–C_{12}) at the expense of the heaviest hydrocarbons. The gasoline selectivity increased in the order USY-500 < USY-720 < HMOR < HBeta < HZSM-5. Moreover, an increase in C_2–C_4 hydrocarbons paralleling the increase in gasoline was also noted on addition of the zeolite co-catalyst. The excess of C_2–C_4 products observed for the hybrid catalysts with respect to the base FT catalyst was due to cracking of primary FT products, as we verified in an additional experiment using the zeolite placed below the Co/SiO_2 in a stacked-bed configuration instead of a physical mixture of both components. Under the reaction conditions used, no aromatic hydrocarbons were detected in the reaction products with both the base and hybrid catalysts. In contrast, gasoline-range aromatics were the predominant hydrocarbons formed at 310 °C over HZSM-5 when an iron-based FT catalyst, highly selective toward C_2–C_4 olefins, was used as the base FT component of the hybrid catalysts [14]. In the present study, the products obtained with the hybrid systems contained almost exclusively linear and branched aliphatic hydrocarbons. It should be emphasized that only very

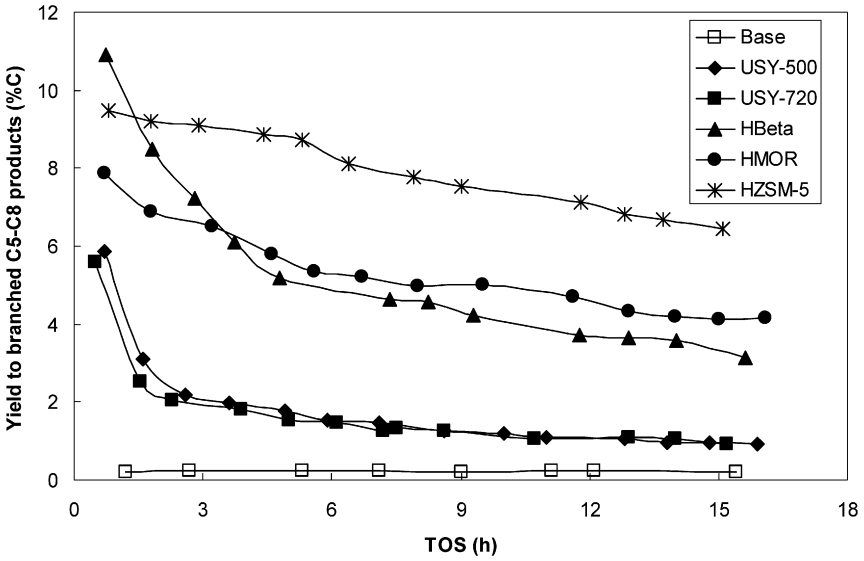

Fig. 4. Evolution of the yield (% C) to branched hydrocarbons in the C_5–C_8 fraction with TOS for the base and hybrid catalysts. Reaction conditions: 250 °C, 2.0 MPa, H_2/CO molar ratio of 2, GHSV of 13.5 $l_{syngas}/(g_{cat}\ h)$.

small amounts of branched products were formed over the base Co/SiO_2 catalyst alone.

The results in Table 5 show that the increase in gasoline selectivity for the different hybrid catalysts, which should provide an indirect measure of the zeolite cracking activity, did not follow the expected trend according to the number and strength of the Brønsted acid sites in the different zeolites (Table 4). In fact, the highest increase was found for the HZSM-5 zeolite, which had fewer Brønsted acid sites than USY-500 and HMOR. This can be explained by considering the effect of water on zeolite activity and the different coking tendencies, as we discuss later.

3.2.2. Evolution of cracking activity with TOS

For the sake of simplicity, we discuss the cracking behavior of the zeolite co-catalyst on the basis of changes in the composition of the C_5–C_8 fraction obtained from the online analyses. Because almost no branched hydrocarbons were produced over the base catalyst alone, the yield to branched products (including paraffins and olefins) in the C_5–C_8 fraction was considered an indirect measure of the zeolite cracking activity. The yield of branched C_5–C_8 products was calculated as follows:

$$\text{Yield iso-}C_{5-8}(\%\ \text{C}) = \frac{(\text{gr C/h})_{\text{iso-}C_{5-8}}}{(\text{gr C/h})_{CO_{\text{inlet}}}} \times 100.$$

The change in the yield of branched C_5–C_8 hydrocarbons with TOS is shown in Fig. 4. Very low yields of these products were obtained for the base catalyst (ca. 0.2% C) during the entire experiment. The formation of branched hydrocarbons drastically increased on addition of the zeolite co-catalyst, particularly at the initial reaction stages. For all zeolites studied, a decrease in the iso-C_{5-8} yield with TOS was demonstrated, suggesting a gradual loss in zeolite cracking activity with reaction time. The results in Fig. 4 clearly show significant differences in the initial yield to branched C_5–C_8 hydrocarbons and in deactivation behavior depending on the particular zeolite topology. The initial yield to branched hydrocarbons, extrapolated from the yield-TOS curves at TOS = 0, decreased in the order HBeta (13.5% C) > HZSM-5 (9.7% C) > HMOR (8.8% C) > USY-500 (8.0% C) > USY-720 (7.1% C), which did not follow the Brønsted acidity trends (Table 4). The relatively low initial yield obtained for USY-500 is particularly surprising, because this had the highest density of Brønsted acid sites. Later, this point is further discussed in light of the *n*-hexadecane cracking experiments.

As shown in Fig. 4, the deactivation rate decreased in the order USY-720 ∼ USY-500 > HBeta > HMOR > HZSM-5. Thus, the large-pore USY and HBeta zeolites with a tridirectional system of interconnected channels deactivated faster than the large-pore HMOR with a monodirectional pore system (excluding the 8-MR pores, which are not accessible for the hydrocarbon molecules), whereas the medium-pore HZSM-5 sample had the lowest deactivation rate. Among the two large-pore 3D samples, the USY zeolites containing the largest cavities (supercages) were more rapidly deactivated than HBeta. Surprisingly, the two USY samples had very similar deactivation trends despite the large differences in Brønsted acidity (Table 4). This result indicates that under the reaction conditions used here, deactivation of the zeolite co-catalyst during the in situ conversion of primary FT products was governed mainly by the pore structure rather than by the acidity.

3.2.3. Amount and nature of the carbonaceous deposits in spent zeolites

The total amount and type (see Section 2) of the carbonaceous deposits remaining on the zeolite at the end of the different experiments are presented in Table 6. In the case of USY-500, an additional experiment was performed in which the reaction was stopped after 3 h TOS to determine the amount and nature of the coke formed on this zeolite during the initial reaction stage, where most of the cracking activity was lost (Fig. 4). The data corresponding to this experiment also are included in

Table 6
Total amount (% C) and type of the carbonaceous deposits in spent zeolites

Zeolite	TOS (h)	C content (wt%)	CH_2Cl_2-soluble coke (wt%)		Type I/ Type II ratio
			Type I	Type II	
USY-500	3.0	8.6	12.3	87.7	0.14
USY-500	15.9	11.3	15.7	84.3	0.19
USY-720	15.2	10.8	23.1	76.9	0.30
HBeta	15.6	10.0	13.4	86.6	0.16
HMOR	16.1	7.1	39.5	60.5	0.65
HZSM-5	15.1	1.9	83.0	17.0	4.95

Table 6. Clearly, the total amount of carbon (determined by elemental analysis) on the spent samples was higher (ca. 10–11 wt%) for the large-pore tridirectional USY and HBeta zeolites than for the large-pore monodirectional HMOR (7.1 wt%), but much lower for the medium-pore HZSM-5 (1.9 wt%). These values are in good agreement with the deactivation trends observed in Fig. 4. It must be noted that the total amount of carbon was similar for the two USY samples despite the large differences in acidity. It is also interesting to note that most of the coke present in the USY-500 sample (representing about 76% of the total) was formed during the first 3 h TOS, which concurs with its relatively rapid initial deactivation, as shown in Fig. 4.

Besides the total amount of carbon, significant differences in the type of soluble coke (no insoluble coke was found) also were seen depending on the zeolite structure. As shown in Table 6, the type I/type II soluble coke ratio decreased in the order HZSM-5 > HMOR > USYs ∼ HBeta, which, taking into account the total carbon content, indicated that the amount of type II soluble coke increased with the dimensions of the intrazeolitic pores. Again, the relative proportion between type I and type II soluble coke did not vary significantly with the Brønsted acidity of the USY zeolite.

The nature of the carbonaceous species retained on the zeolite after the catalytic reaction was studied by GC-MS. The results showed that type I soluble coke, most likely located close to the external surface of zeolite crystallites, constituted mainly long-chain *n*-paraffins (waxes), which are primary products of the FT reaction over the base Co/SiO_2 catalyst. As an example, Fig. 5a shows the chromatogram corresponding to the GC-MS analysis of the type I soluble coke obtained for the experiment with the hybrid catalyst containing the HMOR zeolite. Because the chain length of the adsorbed *n*-paraffins could not be unambiguously determined by mass spectrometry, the type I coke reclaimed in CH_2Cl_2 was also analyzed by simulated distillation (SIMDIS, using a Varian 3800), revealing the presence of C_{20}–C_{60} *n*-paraffins with a near-Gaussian distribution having a maximum centered at C_{35}–C_{40}. The low volatility of the long-chain *n*-paraffins under our reaction conditions would cause their retention on the zeolite surface. In the case of USY and HBeta samples, minor amounts of aromatic compounds (mainly alkylnaphthalenes) were also detected by GC-MS in type I coke. These aromatic molecules likely were retained on the external surface and/or at the entrances of the 12-MR pores

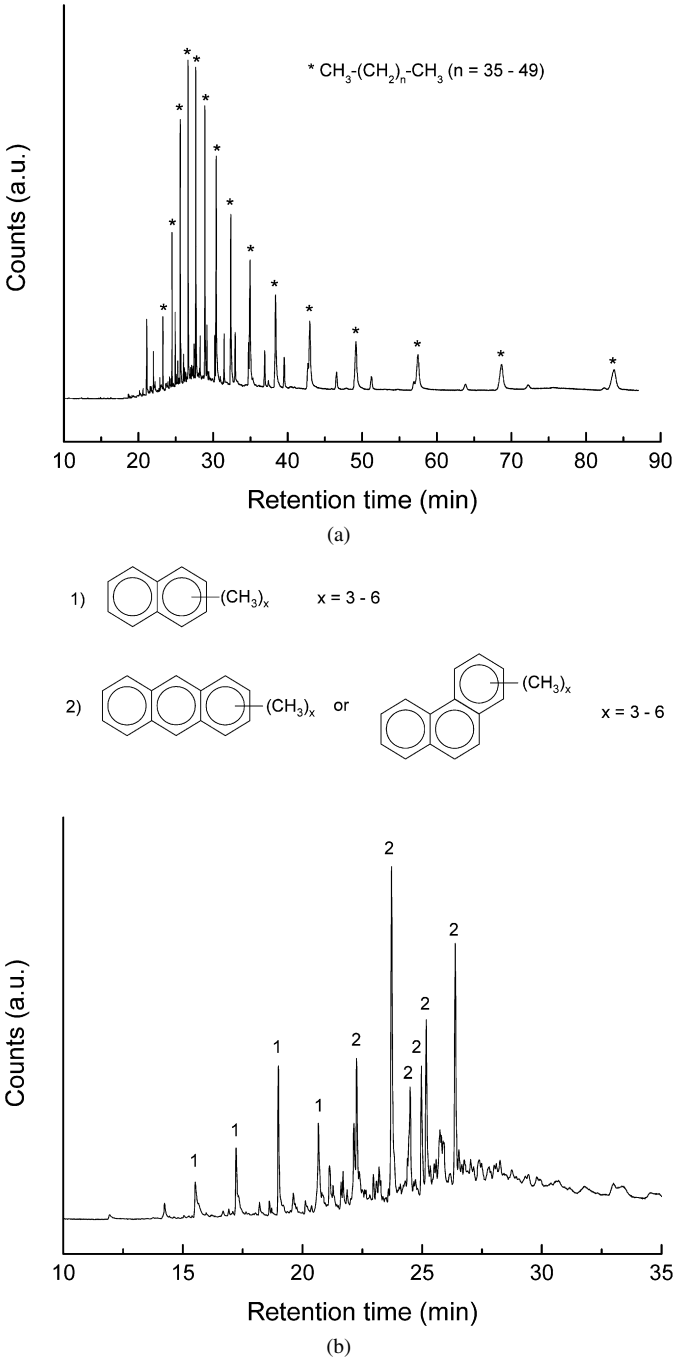

Fig. 5. Chromatogram and assignation of the main compounds in CH_2Cl_2-soluble coke extracted from the used HMOR zeolite after 16 h on stream: (a) type I soluble coke, and (b) type II soluble coke.

because they could be easily extracted during the Soxhlet treatment.

In contrast, type II soluble coke formed in the large pore HMOR, HBeta, and the two USY zeolites contained as major compounds substituted naphthalenes and phenanthrenes with total carbon atoms ranging from 13 to 20. Fig. 5b presents a GC-MS chromatogram of the type II coke formed in the HMOR zeolite with the assignations of the major peaks as an example. The formation of polyaromatic coke during the in situ cracking of primary FT products at 250 °C and 2.0 MPa likely occurs

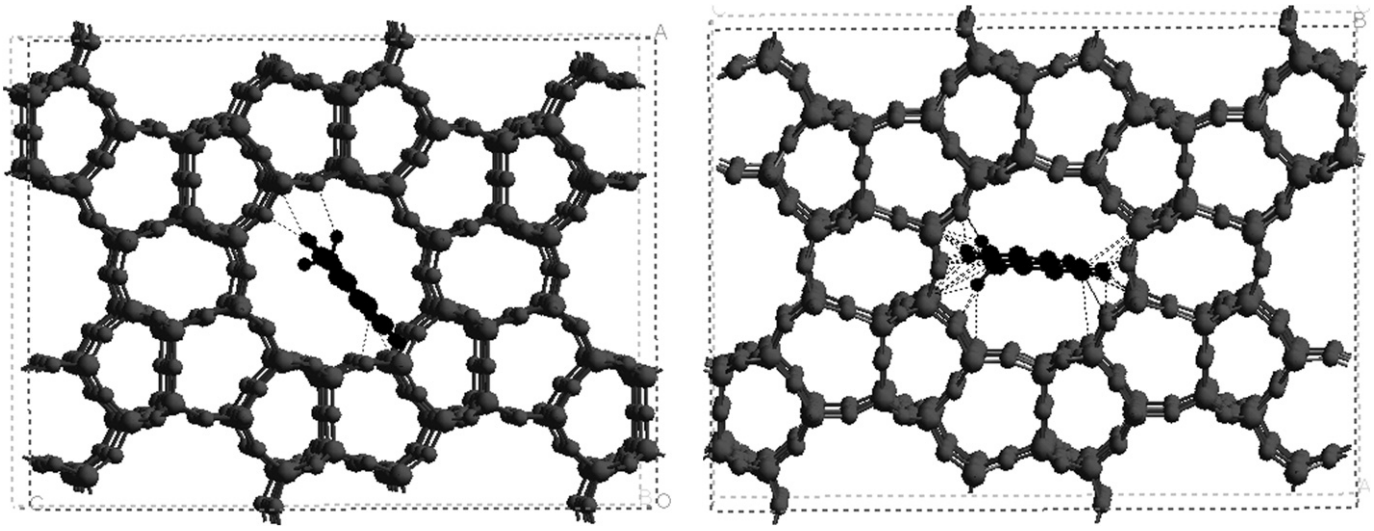

(a) (b)

Fig. 6. Molecular docking simulation results of 1-methylnaphthalene located at the intersection of the two 10-MR channels (a) and in the straight 10-MR pore system (b) of the MFI structure. The dotted lines indicate the van der Waals interactions between the aromatic and the zeolite walls.

through the oligomerization of olefins produced on the Co/SiO_2 FT catalyst, followed by consecutive cyclization and dehydrogenation steps, as occur during conventional catalytic cracking [33,34]. These reactions involve bimolecular hydrogen transfer steps requiring bulkier intermediates than for cracking [35] and that can hardly be accommodated within the narrower pores of HZSM-5. Along with having transition state shape selectivity, the pores of the MFI zeolite are expected to impose serious restrictions on the diffusion of alkylnaphthalenes, the most abundant aromatic molecules found in type II soluble coke in large-pore zeolites and almost absent in HZSM-5.

To confirm this hypothesis, a molecular docking simulation study of 1-methylnaphthalene (taken as representative of the alkylnaphthalenes) within the pores of the MFI structure was performed. The study was carried out using the Cerius4.6 (Accelrys Inc.) software to estimate the Van der Waals interactions between the aromatic molecule and the zeolite walls in the state of minimum energy. These results showed that even if 1-methylnaphthalene could be accommodated at the intersections of the two 10-MR channels (Fig. 6a), it could hardly diffuse out of the pores through the straight 10-MR pore system of the MFI structure, in which the number of interactions (dotted lines) is very high (Fig. 6b). Because the diffusion limitations are expected to be even higher in the sinusoidal 10-MR channels, it can be concluded that alkylnaphthalenes (and bulkier aromatics) can be formed only on the acid sites located at the external surface of the HZSM-5 zeolite. This agrees well with the much lower amount of type II CH_2Cl_2-soluble coke found in this zeolite (Table 6).

FTIR spectroscopy is commonly used to study the nature of the coke molecules and its effect on the acidic properties of the coked zeolites [36–39]. Here this technique was applied, in combination with pyridine adsorption, to study the acidity of the spent USY-500 and HZSM-5 samples previously pretreated at 400 °C under vacuum. The results revealed the presence of several bands at about 1600 cm^{-1} characteristic of the ν_{C-C} vibration of C=C bonds in aromatic rings in the USY-500 sample (not shown), whereas these bands were almost absent in the coked HZSM-5 sample, in agreement with the GC-MS data discussed earlier. Moreover, the density of total Brønsted acid sites (those retaining pyridine at 250 °C) in the used HZSM-5 pretreated at 400 °C was decreased by only ca. 20% with respect to the fresh zeolite, but it strongly decreased by about 80% for USY-500, as shown in Fig. 7. These results suggest that the polyaromatic compounds present in the coke of USY-500 (and in the other large-pore zeolites used) were strongly retained within the micropores blocking the access of pyridine molecules to the acid sites. In contrast, the heavy *n*-paraffins retained on the surface of used HZSM-5 due to their low volatility at 250 °C and 2.0 MPa were mostly removed during pretreatment, making most of the acid sites accessible to pyridine. Thus, the high catalytic stability observed for the hybrid catalyst containing the HZSM-5 zeolite can be explained by the absence of polyaromatic coke inside the micropores and suggests that the *n*-paraffins were retained mainly on the external

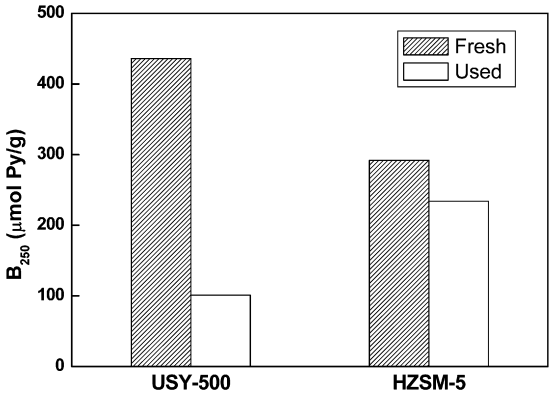

Fig. 7. Number of Brønsted acid sites (μmol/g) retaining pyridine at 250 °C in the fresh and used USY-500 and HZSM-5 zeolites as determined by IR-pyridine experiments.

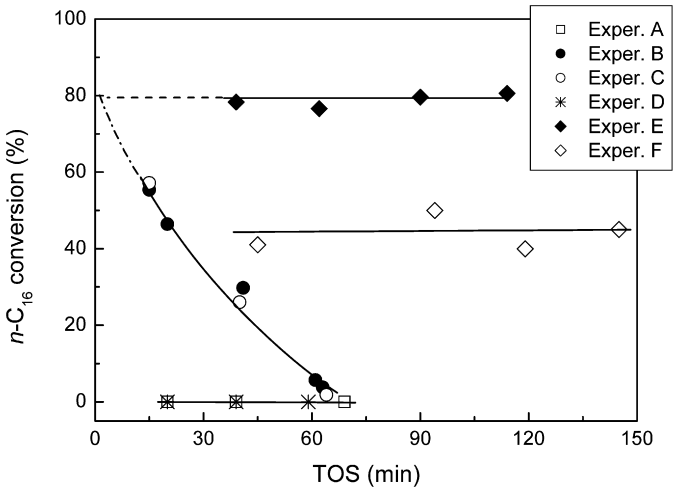

Fig. 8. Conversion–TOS data obtained in the *n*-hexadecane cracking under simulated FT conditions (see Table 1 for the particular conditions used in experiments A–F).

surface, allowing most of the Brønsted acid sites to remain accessible for cracking.

3.3. Cracking of n-hexadecane

Additional experiments performed using n-C_{16} as model molecule yielded interesting findings regarding the activity and stability of the zeolite in hybrid catalysts during the FT reaction. The conversion-TOS curves obtained in the different experiments (see Table 1 for experimental conditions) are shown in Fig. 8. Experiments A–E were carried out in the absence of water in the feed. As revealed by experiment A, no conversion was observed in the absence of any catalyst (reactor charged only with inert SiC), indicating that the contribution of thermal cracking was negligible under the reaction conditions used here. When the reactor was loaded with 1.0 g of HZSM-5 zeolite and in the presence of H_2 in the feed mixture (experiment B), a significant n-C_{16} conversion (ca. 55%) was obtained after 15 min TOS, but the activity rapidly declined with TOS thereafter, reaching a conversion level of about 5% after 60 min TOS. Interestingly, the same behavior was observed when hydrogen was replaced by nitrogen (experiment C). Dissociation of molecular hydrogen on metal-free zeolites at moderate temperatures has been demonstrated by, for instance, H_2–D_2 exchange experiments [40]. Hydrogen activated on purely acidic zeolites was shown to affect selectivity during the catalytic cracking of *n*-heptane even at temperatures as low as 270 °C and 2.4 MPa total pressure [41,42], which are close to the reaction conditions used in the present study. Those authors observed an increase in the *n*-heptane reaction rate with increasing the H_2 partial pressure, and proposed that H_2 activated on the zeolite interacts with the adsorbed olefins (carbenium ions), saturating them and restoring the original Brønsted acid site. Such saturation of the intermediate olefinic products would lead to a decreased deactivation rate by hydrogenating coke precursors. However, the result of experiment C indicates that under our reaction conditions, the purely acidic HZSM-5 zeolite was not able to activate hydrogen.

In experiment D, the reactor was loaded only with the Co/SiO_2 FT catalyst, and the reaction was performed in the presence of H_2. As shown in Fig. 8, almost no conversion was obtained under these conditions, signifying, as expected, that Brønsted acid sites are necessary to crack the *n*-paraffin feed molecules. In this experiment, very small amounts of C_1 and C_2 products (totaling <0.01 wt%) formed through hydrogenolysis on the metal Co sites were detected as the only reaction products. More relevant were the results obtained when a physical mixture of the HZSM-5 zeolite (1.0 g) and the Co/SiO_2 FT catalyst (1.0 g) was loaded into the reactor, thus simulating the hybrid catalysts used in FT study. In this case, a high (ca. 80%) and stable conversion with time, at least within the range of TOS studied, was attained (experiment E). It is noteworthy that almost the same initial n-C_{16} conversion was obtained in experiment C, in which the reactor was loaded only with the acidic zeolite if the conversion-TOS curves for experiments C and E were extrapolated at zero TOS (dashed lines in Fig. 8), suggesting that the FT catalyst did not contribute to the initial activation of the *n*-alkane, in agreement with the outcome of experiment D. The Co/SiO_2 component in the hybrid catalysts likely served as a source of hydrogen activated on the surface metal Co sites and spilled over onto the adjacent zeolite particles. There, the olefinic intermediates (i.e., coke precursors) adsorbed on the zeolite Brønsted acid sites were rapidly hydrogenated and desorbed as alkanes while regenerating the acid sites, which then became available for new catalytic cycles. The hydrogenation of olefinic intermediates can be inferred from the olefin-to-paraffin (O/P) ratio in the cracked products. For instance, the O/P ratio in the C_4 fraction was about 0.3 in the experiment with only zeolite in the catalyst bed (at TOS = 15 min), but was 0 for the physical mixture of zeolite and Co/SiO_2 at any TOS.

Finally, the affect of water on the activity and stability of the zeolite can be inferred from the results obtained in experiment F. As shown in Fig. 8, the presence of water in the feed mixture reduced the activity of the zeolite in the hybrid catalyst by about 45% but had no appreciable effect on zeolite stability. This latter observation indicates that the supply of activated hydrogen from metallic Co sites was still high enough to prevent the rapid buildup of coke precursors on the zeolite acid sites. In fact, no olefins were detected in the cracked products, as occurred in the equivalent experiment in the absence of water. On the other hand, due to its polar nature, water molecules are expected to adsorb on the acidic OH groups of the zeolite. Indeed, Corma et al. recently observed by IR spectroscopy that water interacted with the bridging OH groups of a USY zeolite at temperatures below 350 °C [43]. Thus, it is likely that under our reaction conditions (250 °C, 20 bar total pressure), water competed with the n-C_{16} molecules for adsorption on the zeolite acid sites, thus decreasing the amount of sites available for cracking the *n*-alkane feed and resulting in decreased conversion, as determined experimentally in this work.

By linking the results of the *n*-hexadecane study with those obtained in the FT synthesis over the hybrid catalysts, it can be concluded that, even though the presence of water produced on the Co catalyst during the FT synthesis reduced the cracking

activity of the zeolite, it had no apparent effect on the deactivation behavior. Therefore, the loss of activity of the zeolite observed during the FT experiments is caused by the accumulation of carbonaceous deposits, the amount and nature of which depend mainly on the zeolite structure rather than on acidity, as concluded from this work. On the other hand, the FT study demonstrated that the initial (at TOS = 0) yield to branched hydrocarbons did not correlate with the zeolite Brønsted acidity. Of particular significance is the unexpectedly low initial yield displayed by the USY-500 zeolite, which has the highest density of Brønsted acid sites. This finding can be explained by taking into account the detrimental effect of water on zeolite activity. Indeed, the interaction of water with the zeolite acid sites is expected to be more intense with increasing hydrophilicity of the zeolite [43]. Then the higher the density of framework Al atoms (i.e., the lower the framework Si/Al ratio), the more hydrophilic the zeolite, and a more favorable competition of water with respect to the *n*-alkane feed molecules for adsorption on the zeolite acid sites can be expected. Therefore, the interaction of water would be more intense for the USY-500 sample with the lowest framework Si/Al ratio (Table 3) with respect to the more dealuminated USY-720 and, thus the presence of water in the feed would lead to a greater decrease in activity for cracking the *n*-alkane molecules in the former zeolite. Along with the hydrophilic–hydrophobic character of the zeolite, the intrinsic cracking activity of the acid sites may vary depending on the particular zeolite topology; this effect also should be considered to explain the lack of correlation between the initial yield to branched products and total Brønsted acidity of the zeolite.

4. Conclusion

Acid zeolites with different framework topologies present in hybrid Co/SiO_2-zeolite (50:50 wt/wt) catalysts were active for cracking heavy FT products (mainly long-chain *n*-paraffins) into mainly gasoline-range branched hydrocarbons under typical FT reaction conditions (250 °C, 2.0 MPa, $H_2/CO = 2$). Independent *n*-hexadecane cracking experiments performed under simulated FT conditions revealed that hydrogen activated on the metallic Co sites of the base FT catalyst and spilled over onto the adjacent zeolite particles helped desorb olefinic intermediates, and that the presence of water in the feed reduced the cracking activity of the zeolite by competing with the *n*-alkane adsorption on the zeolite acid sites without affecting its stability with TOS. The competition for adsorption will be more favorable for the polar water molecules as the hydrophilicity of the zeolite is increased, and thus its effect on the zeolite cracking activity will depend on the hydrophilic/hydrophobic character of the zeolite. This fact, along with the differences in the intrinsic strength of the Brønsted acid sites depending on the particular zeolite topology, explains the observed lack of correlation between the initial yield of branched gasoline-range products and the zeolite Brønsted acidity.

Despite the fact that no apparent deactivation was observed in the model *n*-C_{16} experiments with the hybrid catalyst, a gradual loss of activity with TOS was observed in all cases under real FT conditions where light olefins formed on the FT cobalt catalyst were also present, together with *n*-paraffins, in the reaction medium. The total amount of coke deposited on the zeolite after ca. 15–16 h TOS correlated with the observed deactivation rate, and both parameters increased with increasing pore dimensions of the zeolite in the order HZSM-5 < HMOR < HBeta < USYs. Moreover, the coke found in the large-pore zeolites was mainly of aromatic nature (mostly alkylnaphthalenes and alkylphenanthrenes), probably formed from the light FT olefins through consecutive oligomerization, cyclization, and dehydrogenation steps on the zeolite acid sites. In contrast, most of the coke found in HZSM-5 was composed of long-chain *n*-paraffins, which, due to their low volatility under FT conditions, were retained mostly on the zeolite external surface. These differences in the total amount and nature of the carbonaceous deposits between the medium-pore and the large-pore zeolites causes that ca. 80% of the initial Brønsted acid sites were still accessible to pyridine in the spent HZSM-5, whereas only a few acid sites remained available in the spent USY-500 sample. Finally, it should be mentioned that no significant differences in the amount and nature of coke and in the deactivation trends were found for two USY samples displaying quite distinct acidic properties (USY-500 and USY-720).

Acknowledgments

A.M., M.A.A., and J.R. acknowledge the Comisión Interministerial de Ciencia y Tecnología of Spain (CICYT, project CTQ2004-02510/PPQ) for financial support. The authors thank Dr. G. Sastre for performing the molecular docking simulation study and Prof. V. Fornés for providing the FTIR spectroscopic characterization.

References

[1] B.H. Davis, Top. Catal. 32 (2005) 143.
[2] E. Iglesia, Appl. Catal. A 161 (1997) 59.
[3] S. Li, S. Krishamoorthy, A. Li, G.D. Meitzner, E. Iglesia, J. Catal. 206 (2002) 202.
[4] R.A. Store, C.B. Murchison, Hydrocarbon Process. 1 (1982) 147.
[5] S.T. Sie, M.M.G. Senden, H.M.H. van Wechum, Catal. Today 8 (1991) 371.
[6] X. Dupain, R.A. Krul, M. Makkee, J.A. Moulijn, Catal. Today 106 (2005) 288.
[7] X. Dupain, R.A. Krul, C.J. Schaverien, M. Makkee, J.A. Moulijn, Appl. Catal. B 63 (2006) 277.
[8] C.D. Chang, W.H. Lang, A.J. Silvestre, J. Catal. 56 (1979) 268.
[9] V. Udaya, S. Rao, R.J. Gormley, Catal. Today 6 (1990) 207.
[10] H. Nguyen-Ngoc, K. Moller, M. Ralea, Stud. Surf. Sci. Catal. 18 (1984) 291.
[11] N. Guan, Y. Liu, M. Zhang, Catal. Today 30 (1996) 207.
[12] F.G. Botes, Appl. Catal. A 284 (2005) 21.
[13] N.O. Egiebor, W.C. Cooper, Appl. Catal. 55 (1989) 47.
[14] A. Martínez, C. López, Appl. Catal. A 294 (2005) 251.
[15] N. Tsubaki, Y. Yoneyama, K. Michiki, K. Fujimoto, Catal. Commun. 4 (2003) 108.
[16] X. Li, K. Asami, M. Luo, K. Michiki, N. Tsubaki, K. Fujimoto, Catal. Today 84 (2003) 59.
[17] Z.-W. Liu, X. Li, K. Asami, K. Fujimoto, Catal. Commun. 6 (2005) 503.
[18] D. Schanke, S. Vada, E.A. Blekkan, A.M. Hilmen, A. Hoff, A. Holmen, J. Catal. 156 (1995) 85.

[19] R.C. Reuel, C.H. Bartholomew, J. Catal. 85 (1984) 63.
[20] R.D. Jones, C.H. Bartholomew, Appl. Catal. 39 (1988) 77.
[21] A. Martínez, C. López, F. Márquez, I. Díaz, J. Catal. 220 (2003) 486.
[22] A. Corma, V. Fornés, A. Martínez, ACS Symp. Ser. 368 (1988) 542.
[23] C.A. Emeis, J. Catal. 141 (1993) 347.
[24] P. Concepción, C. López, A. Martínez, V.F. Puntes, J. Catal. 228 (2004) 321.
[25] P. Magnoux, P. Roger, C. Canaff, V. Fouche, N.S. Gnep, M. Guisnet, Stud. Surf. Sci. Catal. 34 (1987) 317.
[26] J. Panpranot, S. Kaewkun, P. Praserthdam, J.G. Goodwin Jr., Catal. Lett. 91 (2003) 95.
[27] S. Sun, N. Tsubaki, K. Fujimoto, Appl. Catal. A 202 (2000) 121.
[28] A. Corma, V. Fornés, A. Martínez, J. Sanz, ACS Symp. Ser. 375 (1988) 17.
[29] N.O. Egiebor, W.C. Cooper, B.W. Wojciechovski, Appl. Catal. 55 (1989) 47.
[30] J.P. Van Berge, J. Van De Loosdrecht, S. Barradas, A.M. Van Der Kraan, Catal. Today 58 (2000) 321.
[31] E. Van Oteen, M. Caléis, M.E. Dry, J. Van De Loosdrecht, E.L. Viljoen, J.L. Visagie, J. Phys. Chem. B 109 (2005) 3575.
[32] N.O. Egiebor, W.C. Cooper, B.W. Wojciechovski, Appl. Catal. 55 (1989) 47.
[33] K.A. Cumming, B.W. Wojciechovski, Catal. Rev. Sci. Eng. 38 (1996) 101.
[34] M. Guisnet, P. Magnoux, Appl. Catal. A 212 (2001) 83.
[35] W.O. Haag, R.M. Lago, P.B. Weisz, Faraday Discuss. Chem. Soc. 72 (1982) 317.
[36] H.G. Karge, Stud. Surf. Sci. Catal. 58 (1991) 531.
[37] J.A. Lercher, C. Gründling, G. Eder-Mirth, Catal. Today 27 (1996) 353.
[38] C.L. Li, O. Novaro, E. Muñoz, J.L. Boldú, X. Bokhimi, J.A. Wang, T. López, R. Gómez, Appl. Catal. A 199 (2000) 211.
[39] H.S. Cerqueira, P. Ayrault, J. Datka, P. Magnoux, M. Guisnet, J. Catal. 196 (2000) 149.
[40] J. Nováková, L. Kubelková, B. Wichterlová, T. Justa, Z. Dolejsek, Zeolites 2 (1982) 17.
[41] J. Meusinger, A. Corma, J. Catal. 152 (1995) 189.
[42] J. Meusinger, A. Corma, J. Catal. 159 (1996) 353.
[43] A. Corma, O. Marie, F.J. Ortega, J. Catal. 222 (2004) 338.